Simulation of the CsI crystal calorimeter of the detector of tau-charm factory in Novosibirsk

V.L. Ivanov*, I.S. Bulyzhenkov, D.A. Epifanov, A.S. Kuzmin, B.A. Shwartz, E.S. Prokhorova, S.B. Oreshkin, Yu.V. Yudin, Yu.V. Usov, A.A. Osipov

Budker Institute of Nuclear Physics (Novosibirsk, Russia)

*e-mail: V.L.Ivanov@inp.nsk.su

This work is supported by grant RSF 19-72-20114

Abstract

The poster presents a current status of the simulation of the CsI crystal calorimeter of the detector of charm-tau factory in Novosibirsk. The calorimeter employs the scheme with the crystals focusing at the beams interaction point to obtain the optimal energy and coordinate resolutions. To avoid the «dead zones» effect, a slight defocusing in longitudinal and transversal directions is made. The description of the fully parametrized crystal geometry generator is presented. Using this generator the optimization of the calorimeter geometry parameters was done. The report also presents the results for the coordinate and energy correction functions calculation, as well as the estimation of the resulting energy and coordinate resolutions. Finally, the influence of the dead material in front of the calorimeter was studied.

1. Pure CsI calorimeter for charm-tau factory detector

- The main option for the calorimeter of the charm-tau factory detector is that based on scintillation crystals of *pure* CsI
- The shape of crystals is truncated pyramid (trapezoid)
- The optimal coordinate resolution can be obtained by the focusing of crystals on the beams interaction point
- However, to avoid a big energy loss at the edges of crystals («dead zones» effect) one should also implement the defocusing of the edges from the interaction point
- The pileup noise becomes significant at high luminosity, especially in the endcap
- The usage of the crystals of pure CsI with short decay time of ~30 ns solves the problem
- The price to pay is a relatively low light yield. To compensate it we plan to use APDs and wavelength shifters

Fig. 1

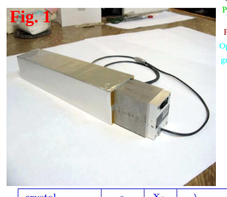

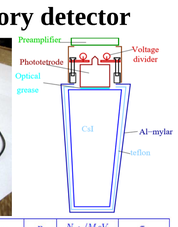

crystal	ρ, g/cm^3	X_0, cm	λ_{em}, nm	n	N_{ph}/MeV	τ, ns
CsI(Tl)	4.51	1.86	550	1.8	52000	1000
CsI	4.51	1.86	305/400	2	5000	30/1000
BaF_2	4.89	2.03	220/310	1.56	2500/6500	0.6/620
CeF_3	6.16	1.65	310	1.62	600	3
$PbWO_4$	8.28	0.89	430	2.2	25	10
$LuAlO_3$(Ce)	8.34	1.08	365	1.94	20500	18
$Lu_3Al_5O_{12}$(Ce)	7.13	1.37	510	1.8	5600	60
Lu_2SiO_5(Ce)	7.41	1.2	420	1.82	26000	12/40

2. Barrel calorimeter geometry

- We choose the distance to the front face of the crystal ON in a way to get the distance from bottom edge of the crystal to the z-axis equal ρ_0
- The main issue is the choice of the set of the angles ψ_i. We require $N_0N_1 = N_0N_2 = d/2$, d – is a parameter, approximately corresponding to the crystal face size on θ
- This gives the geometric progression for the tangents of half angles $\tan(\psi_i/2) = q^i$, where

$$q \equiv \left(\frac{1 - d/2\rho_0}{1 + d/2\rho_0}\right) < 1$$

- The given number N_θ of crystals should fit exactly into the given distance z_0 along z-axis. From that we obtain

$$q = \sqrt[N_\theta]{\sqrt{\left(\frac{z_0}{\rho_0}\right)^2 + 1} - \frac{z_0}{\rho_0}}$$

Fig. 2

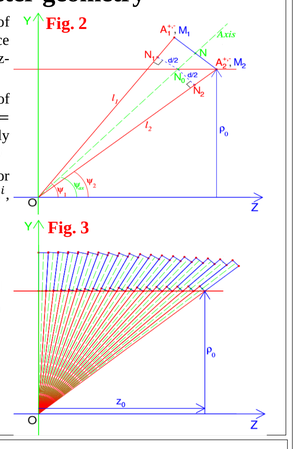

Fig. 3

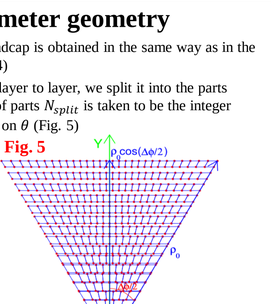

3. Endcap calorimeter geometry

- The set of angles $\gamma_i = \pi/2 - \psi_i$ for the endcap is obtained in the same way as in the barrel with the substitution $z_0 \leftrightarrow \rho_0$ (Fig. 4)
- Since the crystal size on φ increases from layer to layer, we split it into the parts with equal angular size on φ, the number of parts N_{split} is taken to be the integer part of the ratio of crystal size on φ to that on θ (Fig. 5)

Fig. 4

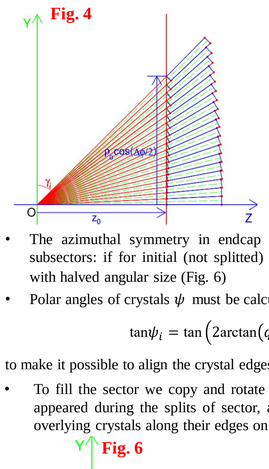

Fig. 5

- The azimuthal symmetry in endcap may be improved by splitting sectors into subsectors: if for initial (not splitted) crystal $N_{split} \geq 4$, it is generated recursively with halved angular size (Fig. 6)
- Polar angles of crystals ψ must be calculated by formula

$$\tan\psi_i = \tan\left(2\arctan\left(q^i\right)\right)\frac{\cos\left(\Delta\varphi/(2N_{subsec})\right)}{\cos(\Delta\varphi/2)}$$

to make it possible to align the crystal edges by the rotation on φ

- To fill the sector we copy and rotate the crystals on φ. The gaps between layers, appeared during the splits of sector, are removed by projection of the vertices of overlying crystals along their edges on the plane of underlying crystals (Fig. 7)

Fig. 6

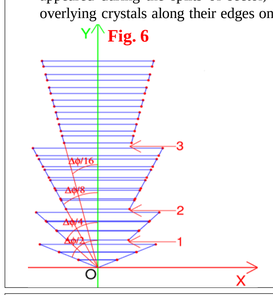

Fig. 7

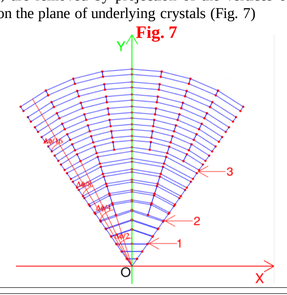

4. Defocusing of crystal edges

- Lines of crystals are defocused in the $r - \varphi$ plane by setting their focusing centers in the vertices of regular polygon with radius of circumscribed circle r_0 (defocusing radius), see Fig. 8
- Central crystal is added to defocus the barrel crystals on θ (Fig. 9). Similar procedure is done for the endcap
- Crystal is wrapped in teflon (0,2 mm) and mylar (0,05 mm) envelopes

Fig. 8

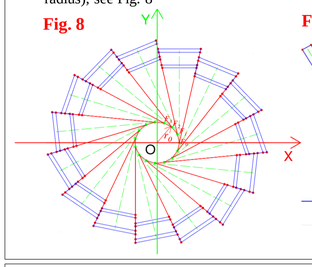

Fig. 9

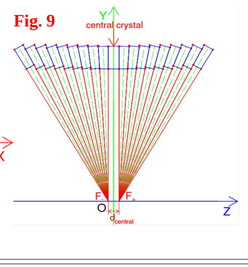

5. Parametrized geometry generator

- Set of optimal geometry parameters is passed to GEANT4 through **DD4hep**:

Parameter	ρ_0, mm	z_0, mm	l_{cryst}, mm	r_0, mm	ρ_{min}, mm	N_φ	N_θ	N_{shapes}
Barrel	1090	1260	330	20	-	114	19	**20**
Endcap	1090	1290	330	20	300	19	19	**33**

- The calorimeter layout with these geometry parameters:

Fig. 10

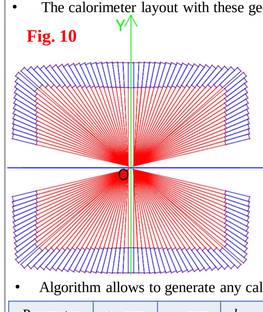

Fig. 11

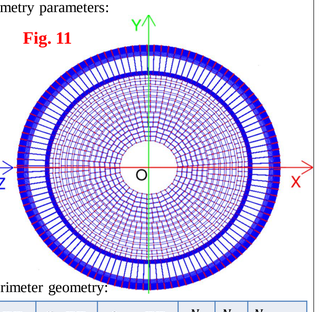

- Algorithm allows to generate any calorimeter geometry:

Parameter	ρ_0, mm	z_0, mm	l_{cryst}, mm	r_0, mm	ρ_{min}, mm	N_φ	N_θ	N_{shapes}
Barrel	1090	1260	1000	400	-	12	3	7
Endcap	1090	1290	1000	100	1	5	5	14

Fig. 12

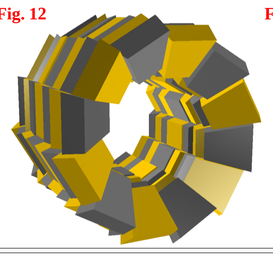

Fig. 13

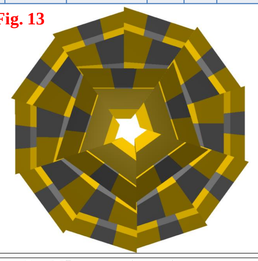

5. Cluster coordinate corrections

- Reconstructed photon angles θ_{rec} and φ_{rec} are concentrated near the crystals centers and are systematically shifted from the true (generated) angles θ_{gen} and φ_{gen}
- Due to the crystal focusing the correlation between φ_{rec} and θ_{rec} appears to be small, and we can define *independent* correction functions $\delta\varphi_{rec}(\varphi_{rec})$and $\delta\theta_{rec}(\theta_{rec})$
- Correction function $\delta\theta_{rec}$ is calculated as the *most probable* value of the difference between generated and reconstructed angles $\delta\theta_{rec}(\theta_{rec}) = \theta_{gen} - \theta_{rec}$ for the given θ_{rec}. This most probable value is found from the gaussian fit near the maximum of $\theta_{gen} - \theta_{rec}$ distribution, see Fig. 22
- Correction function $\delta\theta_{rec}$ (see Fig. 23-24) slightly depends on the photon energy (see Fig. 25)
- The $\delta\theta_{rec}$ and other correction functions are calculated for the set of energies (10, 25, 50, 100, 200, 500, 1000, 2000 and 3500 MeV). For other energies the linear interpolation between these nodes is used

Fig. 22

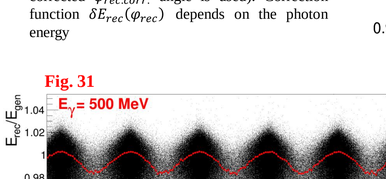

- The correction $\delta\varphi_{rec}$ is calculated similarly to $\delta\theta_{rec}$, but separately in each zone on $|\pi/2 - \theta_{rec}|$, in which the number of crystals on φ is a constant (see Fig. 26)
- $\delta\varphi_{rec}$ is calculated as the most probable value of the difference between generated and reconstructed angles $\delta\varphi_{rec}(\varphi_{rec}) = \varphi_{gen} - \varphi_{rec}$, see Fig. 27. Slight dependence of $\delta\varphi_{rec}$ on the photon energy is also observed

Fig. 26

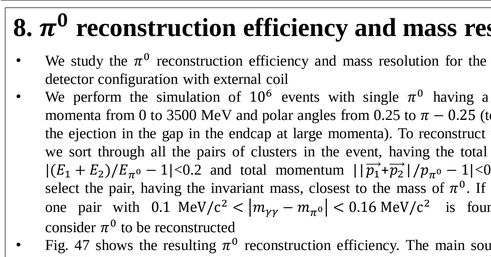

Fig. 27

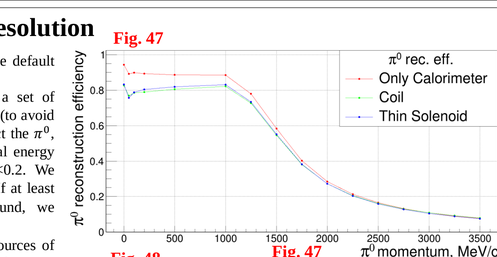

6. Cluster energy corrections

- Correction function $\delta E_{rec}(\theta_{rec})$ is calculated (without application of coordinate corrections) as the most probable value of the ratio $\delta E_{rec}(\theta_{rec}) = E_{rec}/E_{gen}$. This most probable value is found as a maximum of lognormal fit of E_{rec}/E_{gen} distribution, see Fig.
- Correction function $\delta E_{rec}(\theta_{rec})$ depends on the photon energy, see Fig. 30

Fig. 28

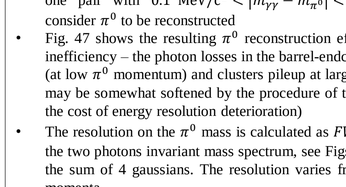

- Correction function $\delta E_{rec}(\varphi_{rec})$ is calculated *after application* of $\delta E_{rec}(\theta_{rec})$ correction as the most probable value of the ratio $\delta E_{rec}(\varphi_{rec}) = E_{rec}/E_{gen}$
- Of course, the largest leakages happen in the gaps between crystals (see Fig. 32, where corrected $\varphi_{rec.corr.}$ angle is used). Correction function $\delta E_{rec}(\varphi_{rec})$ depends on the photon energy

Fig. 29

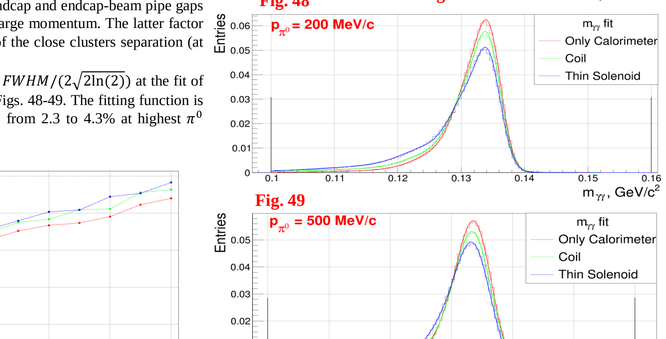

Fig. 30

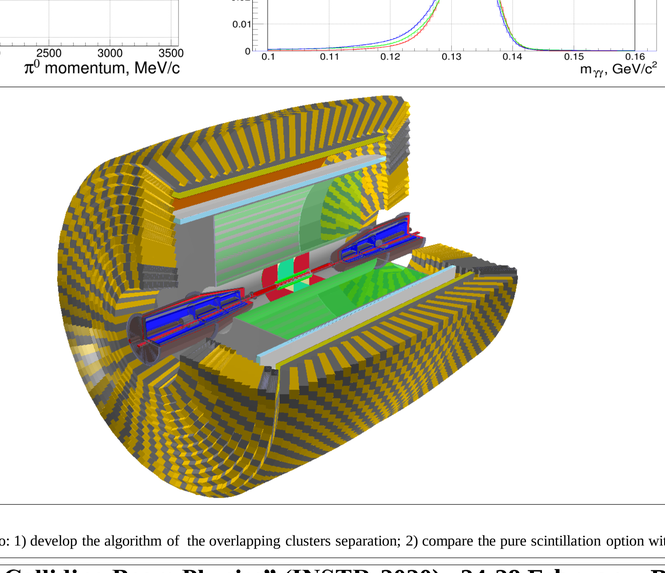

Fig. 31

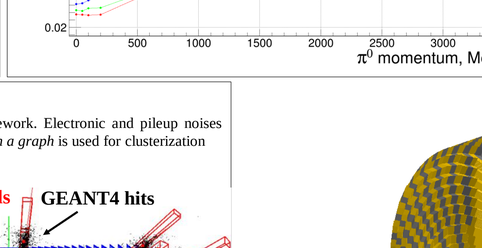

Fig. 32

7. Cluster energy and coordinate resolutions

- We study the photon energy and coordinate resolutions for two detector material layouts. First is the default configuration with the vacuum pipe, TPC, drift chamber and FARICH in front of the calorimeter. The magnetic field of 1 Tl in this configuration is created by the external coil, surrounding the calorimeter. In the second configuration the magnetic field is created by the thin (~0.1 X_0) solenoid, placed between the drift chamber and the FARICH. The amount of the dead material, added by the solenoid, is comparable with that in FARICH (~0.15 X_0)
- The influence of thin solenoid is ambivalent. On the one hand it increases the portion of photons converting in e^+e^- pair before reaching the calorimeter. On the other hand, since there is no magnetic field outside the solenoid, the pairs, produced in the solenoid and FARICH, are not rotated in the magnetic field. So, with the thin solenoid option one should expect the lower cluster splitting probability and the poorer energy resolution (since the e^+e^- pair with lower and fluctuating energy mimic the initial photon). The fraction of e^+e^- pairs, produced in the vacuum tube, TPC and drift chamber in both "coil" and "thin solenoid" configurations is seen as a couple of clusters with comparable energies in different parts of the calorimeter
- We use the configuration without any dead material (only calorimeter) as an ideal reference
- First of all, we simulate $3 \cdot 10^6$ single-photon events with the energies 50, 100, 200, 500, 1000, 2000 and 3500 MeV, uniformly distributed on the polar angle
- For the photons, flying in the barrel, we calculate the ratio of the number of events with the 2 or more reconstructed clusters (seed threshold is 10 MeV) to the events with one cluster, see Fig. 33. We call this ratio the *cluster splitting probability*. It is seen, that it is ~1-3% even for the "only calorimeter" configuration. For thin solenoid option, as expected, it is ~1% smaller, than for the default option with external coil
- For the events with 2 or more clusters Fig. 34 shows the spectrum of the sum of the energies of the minor clusters, i.e. clusters, having the energies lower than the energy of the most energetic cluster
- The study of the energy and coordinate resolutions is performed separately in each ring on θ, see the binning scheme in Fig. 35. *The events with only one reconstructed cluster are used*
- The energy resolutions are calculated as $FWHM/(2\sqrt{2\ln(2)})$ for the fit of the E_{rec}/E_{gen} ratio, see Figs. 36-39. The fit uses the reflected and shifted lognormal with two additional gaussians to describe tails of the distribution.
- The resulting energy resolution for $E_\gamma = 1000$ MeV is shown in Fig. 40. As it was expected, the opposite side of the larger efficiency for thin solenoid option is the poorer energy resolution (at ~15% at 1 GeV compared to the external coil). Another effect is the deformation of the energy spectra at the intermediate energies 200-700 MeV by the e^+e^- pair (see Fig. 37-38), produced in the FARICH and solenoid and mimicking the initial photon

Fig. 33

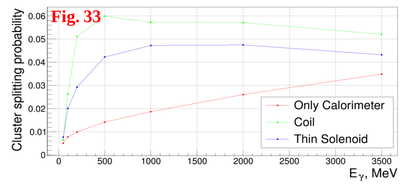

Fig. 34

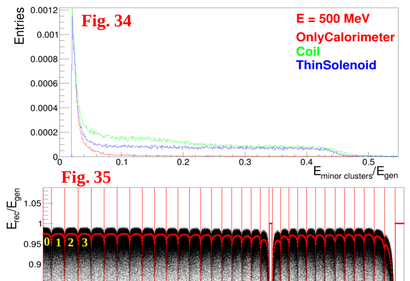

Fig. 35

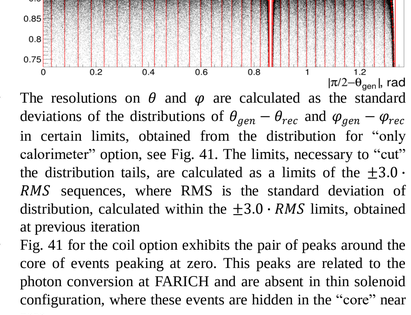

- The resolutions on θ and φ are calculated as the standard deviations of the distributions of $\theta_{gen} - \theta_{rec}$ and $\varphi_{gen} - \varphi_{rec}$ in certain limits, obtained from the distribution for "only calorimeter" option, see Fig. 41. The limits, necessary to "cut" the distribution tails, are calculated as a limits of the $\pm 3.0 \cdot RMS$ sequences, where RMS is the standard deviation of distribution, calculated within the $\pm 3.0 \cdot RMS$ limits, obtained at previous iteration
- Fig. 41 for the coil option exhibits the pair of peaks around the core of events peaking at zero. This peaks are related to the photon conversion at FARICH and are absent in thin solenoid configuration, where these events are hidden in the "core" near zero
- For the given method of calculation of coordinate resolutions we do not see significant differences between coil and thin solenoid options at any energy, see Figs. 42-43

Fig. 36

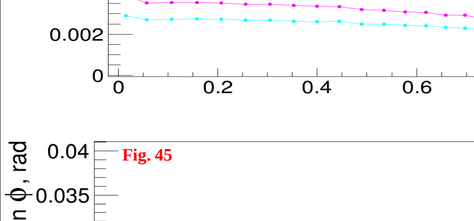

Fig. 37

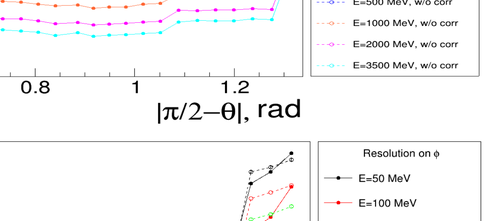

Fig. 38

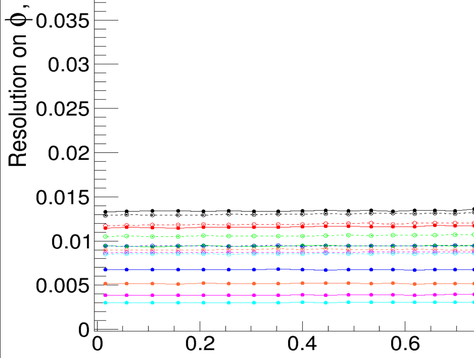

Fig. 39

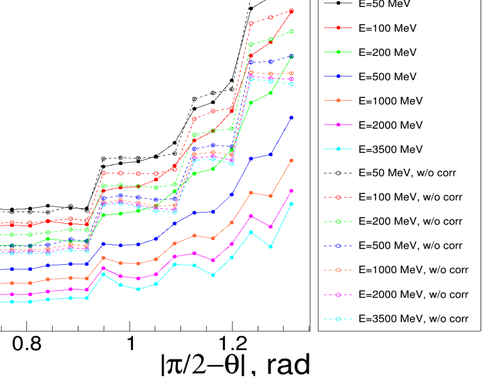

Fig. 40

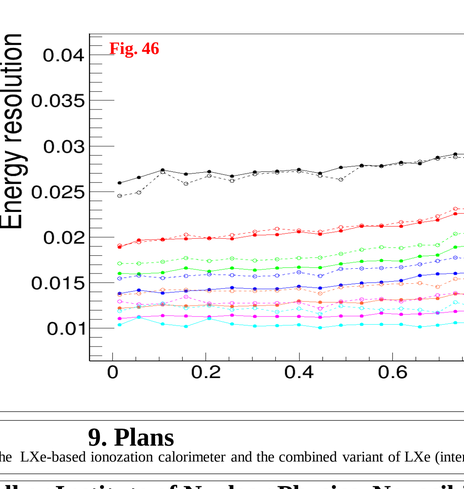

Fig. 41

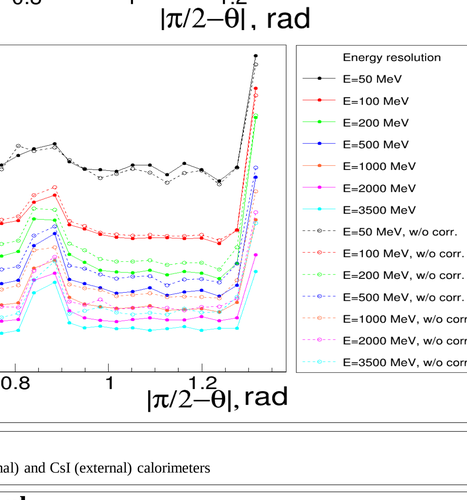

Fig. 42

Fig. 43

- Figs. 44-46 show the coordinate and energy resolutions for the set of photon energies from 50 to 3500 MeV. In order to understand the impact of the coordinate and energy corrections, the resolutions, calculated *without* the corrections are also shown. Generally, the larger energy – the larger effect of the correction on the resolution is seen. The energy correction corrects the mean of the energy deposition with only small improvement of energy resolution

Fig. 44

Fig. 45

Fig. 46

8. π^0 reconstruction efficiency and mass resolution

- We study the π^0 reconstruction efficiency and mass resolution for the default detector configuration with external coil
- We perform the simulation of 10^6 events with single π^0 having a set of momenta from 0 to 3500 MeV and polar angles from 0.25 to $\pi - 0.25$ (to avoid the ejection in the gap in the endcap at large momenta). To reconstruct the π^0, we sort through all the pairs of clusters in the event, having the total energy $|(E_1 + E_2)/E_{\pi^0} - 1|$<0.2 and total momentum $||\vec{p_1}+\vec{p_2}|/p_{\pi^0} - 1|$<0.2. We select the pair, having the invariant mass, closest to the mass of π^0. If at least one pair with $0.1\ \text{MeV/c}^2 < |m_{\gamma\gamma} - m_{\pi^0}| < 0.16\ \text{MeV/c}^2$ is found, we consider π^0 to be reconstructed
- Fig. 47 shows the resulting π^0 reconstruction efficiency. The main sources of inefficiency – the photon losses in the barrel-endcap and endcap-beam pipe gaps (at low π^0 momentum) and clusters pileup at large momentum. The latter factor may be somewhat softened by the procedure of the close clusters separation (at the cost of energy resolution deterioration)
- The resolution on the π^0 mass is calculated as $FWHM/(2\sqrt{2\ln(2)})$ at the fit of the two photons invariant mass spectrum, see Figs. 48-49. The fitting function is the sum of 4 gaussians. The resolution varies from 2.3 to 4.3% at highest π^0 momenta

Fig. 47

Fig. 48

Fig. 49

Fig. 50

6. Clusterization

- Our reconstruction code for the calorimeter is based on the code from FCCSW framework. Electronic and pileup noises addition, zeroes suppression is performed. Algorithm for finding *connected components in a graph* is used for clusterization
- 30 single photons with energy 3.5 GeV:

Fig. 14

Fig. 15

9. Plans

- We plan to: 1) develop the algorithm of the overlapping clusters separation; 2) compare the pure scintillation option with the LXe-based ionozation calorimeter and the combined variant of LXe (internal) and CsI (external) calorimeters